University of Reading

# *Assessing methods to extrapolate the vertical wind-speed profile from surface observations in a city centre during strong winds*

Article

Published Version

Creative Commons: Attribution 4.0 (CC-BY)

Open Access

Kent, C. W., Grimmond, C. S. B., Gatey, D. and Barlow, J. F. (2018) Assessing methods to extrapolate the vertical wind-speed profile from surface observations in a city centre during strong winds. Journal of Wind Engineering and Industrial Aerodynamics, 173. pp. 100-111. ISSN 0167-6105 doi: https://doi.org/10.1016/j.jweia.2017.09.007 Available at https://centaur.reading.ac.uk/73656/

It is advisable to refer to the publisher's version if you intend to cite from the work. See Guidance on citing.

To link to this article DOI: http://dx.doi.org/10.1016/j.jweia.2017.09.007

Publisher: Elsevier

All outputs in CentAUR are protected by Intellectual Property Rights law, including copyright law. Copyright and IPR is retained by the creators or other copyright holders. Terms and conditions for use of this material are defined in the End User Agreement.

University of Reading

www.reading.ac.uk/centaur

**CentAUR**

Central Archive at the University of Reading

Reading's research outputs online

Journal of Wind Engineering & Industrial Aerodynamics 173 (2018) 100–111

Contents lists available at ScienceDirect

Journal of Wind Engineering & Industrial Aerodynamics

journal homepage: www.elsevier.com/locate/jweia

# Assessing methods to extrapolate the vertical wind-speed profile from surface observations in a city centre during strong winds

Christoph W. Kent [a,*], C.S.B. Grimmond [a], David Gatey [b], Janet F. Barlow [a]

[a] Department of Meteorology, University of Reading, Reading, RG6 6BB, United Kingdom
[b] Risk Management Solutions, London, EC3R 8NB, United Kingdom

ARTICLE INFO

*Keywords:*
Aerodynamic roughness length
Morphometric methods
Source area
Urban
Wind
Wind-speed profile
Zero-plane displacement

ABSTRACT

Knowledge of the vertical wind-speed profile in cities is important for the construction and insurance industries, wind energy predictions, and simulations of pollutant and toxic gas release. Here, five methods to estimate the spatially- and temporally-averaged wind-speed profile are compared in London: the logarithmic wind law (*LOG*); the Deaves and Harris equilibrium ($DH_e$) and non-equilibrium ($DH_v$) models; an adaptation of the power law (*PL*) and the Gryning et al. (*GR*) profile. Using measurements at 2.5 times the average building height, a source area model is used to determine aerodynamic roughness parameters using two morphometric methods, which assume homogeneous and variable roughness-element heights, respectively. Hourly-averaged wind speeds are extrapolated to 200 m above the canopy during strong wind conditions, and compared to wind speeds observed with Doppler lidar. Wind speeds are consistently underestimated if roughness-element height variability is not considered during aerodynamic parameter determination. Considering height variability, the resulting estimations with the $DH_e$ and *GR* profiles are marginally more similar to observations than the $DH_v$ profile, which is more accurate than the *LOG* and *PL* methods. An exception is in directions with more homogeneous fetch and a gradual reduction in upwind roughness, where the *LOG* and *PL* profiles are more appropriate.

## 1. Introduction

Modelling the wind-speed profile in the lowest few hundred metres of the urban boundary layer (UBL) is becoming increasingly important. The rapid development of urban areas is resulting in taller buildings with unique forms and arrangements which the construction and insurance industries need to account for (Petrini and Ciampoli, 2012; Tanaka et al., 2012; Taranath, 2016). The threat of pollutant and hazardous material release (accidental and terror related) is increasingly being realized (Belcher, 2005; Tominaga and Stathopoulos, 2016), and widespread city-based renewable wind energy is being explored (Millward-Hopkins et al., 2013; Ishugah et al., 2014; Emejeamara et al., 2015). Accurate vertical profiles of wind-speed are essential boundary conditions to physical (i.e. wind tunnel) and numerical (e.g. computational fluid dynamics) models, as the final results are sensitive to these initial conditions (e.g. Schultz et al., 2005; Ricci et al., 2016). Critical questions which remain include: how well can the spatially- and temporally-averaged urban boundary layer winds be estimated, what are the minimum input requirements, and what are the associated uncertainties?

Over flat, homogeneous terrain with extensive fetch, a dynamic equilibrium between strong winds and the surface roughness is reached, which is well understood and modelled quantitatively (Harris and Deaves, 1980). However, flat homogeneous fetch is rare in urban areas. There are often distinct changes in surface cover in close proximity, characterised by different land cover types and roughness elements of different form (e.g. height variability, density). The structure of the UBL is therefore highly variable because of the numerous sources and sinks of heat and momentum (Gryning et al., 2011), which means that modelling the wind-speed profile is challenging.

The UBL is traditionally divided into several distinct layers (e.g. Fernando, 2010; his Fig. 9), the location of which is determined by surface morphology and mesoscale conditions (Barlow, 2014). The urban canopy layer (UCL) is where surface roughness elements such as buildings are located (Oke, 2007) and is associated with highly variable flow. The UCL is within the roughness sublayer (RSL) (Roth, 2000), the depth of which is typically 2–5 times the average roughness-element height ($H_{av}$) (Roth, 2000; Barlow, 2014), varying with the roughness-element density (Raupach et al., 1991; Grimmond and Oke, 1999; Roth, 2000;

* Corresponding author.
*E-mail addresses:* C.W.Kent@pgr.reading.ac.uk (C.W. Kent), c.s.grimmond@reading.ac.uk (C.S.B. Grimmond).

https://doi.org/10.1016/j.jweia.2017.09.007
Received 20 April 2017; Received in revised form 7 September 2017; Accepted 7 September 2017
Available online 12 December 2017
0167-6105/© 2017 The Authors. Published by Elsevier Ltd. This is an open access article under the CC BY license (http://creativecommons.org/licenses/by/4.0/).

Oke, 2007; Barlow, 2014), staggering (Cheng and Castro, 2002) and height variability (Cheng and Castro, 2002). Between the RSL and approximately 10% of the boundary layer depth is the inertial sublayer (ISL), where the flow becomes free of the wakes associated with individual roughness elements. If the airflow is fully adapted to upwind roughness elements in the ISL, a horizontally homogeneous flow is observed (Barlow, 2014) and it is therefore possible to determine a spatially- and temporally-averaged wind-speed profile.

This paper assesses how well the wind-speed profile can be modelled using surface observations at a reference site in central London, United Kingdom. The aerodynamic roughness parameters of the zero-plane displacement ($z_d$) and aerodynamic roughness length ($z_0$) are determined using two morphometric methods (i.e. from surface form). One morphometric method assumes homogeneous roughness elements (Macdonald et al., 1998; *Mac*), the other considers their height variability (Kanda et al., 2013; *Kan*). Five different methods are then used to extrapolate the wind speed to 200 m above the canopy. These wind speeds are compared to those observed using Doppler lidar.

Specifically, the methods considered are: the logarithmic wind law (Blackadar and Tennekes, 1968) (*LOG*); the Deaves and Harris equilibrium ($DH_e$) and non-equilibrium ($DH_v$) models (Deaves and Harris, 1978; Harris and Deaves, 1980); an adapted power law which directly considers surface roughness (Sedefian, 1980) (*PL*) and a profile proposed by Gryning et al. (2007) (*GR*) (see Section 2 for the selection of methods). Analysis is undertaken for neutral conditions, to allow the accuracy of extrapolated profiles during 'ideal' conditions to be understood first, without the additional uncertainties associated with thermal effects (e.g. Högström, 1996).

## 2. Describing the boundary layer wind speed using surface observations

In addition to the models named above, other methods to describe the spatially- and temporally-averaged wind-speed profile have been derived (Wieringa, 1986; Etling, 2002; Wilson and Flesch, 2003, Emeis et al., 2007; Peña et al., 2010; Yang et al., 2016). Wieringa's (1986) two-layer model requires definition of the height above which the logarithmic wind law (*LOG*) becomes inappropriate. Given that it is both difficult to determine this height in the UBL (e.g. Roth, 2000; Barlow, 2014) and the performance of the *LOG* method is assessed in this study, Wieringa's (1986) method and the two-layer model of Wilson and Flesch (2003) are not considered here. Emeis et al. (2007) developed Etling's (2002) multi-layer model to incorporate the effects of atmospheric stability. As with Wieringa's (1986) model, the applicable height range of *LOG* is required. Additionally, the method requires the geostrophic wind speed (as well as surface measurements) and is therefore not considered here. For similar reasons the Yang et al. (2016) model is not considered. Peña et al. (2010) use Gryning et al.'s (2007) mixing length model with a variety of mixing length parameterisations. However, there is no conclusive evidence that any of the assessed parameterisations provide improved accuracy for wind-speed estimation, therefore only the original formulation of Gryning et al. (2007) is used.

For simplicity, the following assumptions are typically made when modelling the neutral wind-speed profile in the atmospheric boundary layer (e.g. Garratt, 1992): (i) stationarity, (ii) horizontal homogeneity, (iii) a barotropic atmosphere, where density is a function of pressure only, and (iv) uniform roughness with an extensive fetch and no subsidence, therefore there is no mean vertical component of the wind. These assumptions are inherent in each of the five methods assessed here, however $DH_v$ does not assume uniform upwind roughness (assumption iv).

Observations of the vertical wind profile are becoming increasingly available in urban areas (e.g. Tamura et al., 2001; Allwine et al., 2002; Emeis, 2004; Frehlich et al., 2006; Emeis et al., 2007; Drew et al., 2013; Tan et al., 2015; Liu et al., 2017). Especially because remote sensing techniques, such as lidar and sodar, overcome the impracticalities associated with *in-situ* tower mounted (Al-Jiboori and Fei, 2005) or tethersonde (Tsuang et al., 2003) observations. Lidar is often favoured to sodar in urban areas, due to the noisiness of the latter. However, both have been used to assess the structure of the UBL (Barlow et al., 2008, 2011) and associated wind flow (Drew et al., 2013; Lane et al., 2013; Wood et al., 2013; Kent et al., 2017a). Specifically in London, wind speeds observed with Doppler lidar have been used to assess how accurately wind speeds can be: translated from a 'rural' airport site to central London (Drew et al., 2013); and, estimated using the logarithmic wind law extrapolated from observations at approximately 2.5 times the canopy height, using a range of methods to determine $z_d$ and $z_0$ (Kent et al., 2017a). Here this work is further developed by considering wind directions with a more complex fetch, as well as different methods to extrapolate the wind-speed profile. A source area footprint model is used to estimate the upstream effective roughness.

### 2.1. The logarithmic wind law

The logarithmic wind law (*LOG*), may be derived through: (i) matching a region where the velocity gradients determined from equations obeying the upper and lower boundary conditions of ABL flow are the same (also termed asymptotic similarity theory); or (ii) eddy viscosity, or k-theory. The derivation demonstrates that for a height, $z$, if the flow is aligned to the wind direction, the mean wind speed $\overline{U}(z)$ during neutral atmospheric stability can be determined by (Blackadar and Tennekes, 1968; Tennekes, 1973):

$$\overline{U}(z) = \frac{u_*}{\kappa}\ln\left(\frac{z - z_d}{z_0}\right) \tag{1}$$

where $u_*$ is the friction velocity and $\kappa$ is von Karman's constant. Following full scale field observations which indicate $\kappa = 0.38$–$0.42$ and scaled experiments in wind tunnels indicating $\kappa = 0.4$ (Garratt, 1992), a value of $\kappa = 0.4$ is used in this work. The zero-plane displacement ($z_d$) is the vertical displacement of the wind-speed profile due to surface roughness elements and has been demonstrated to correspond to the 'drag centroid' of the surface, or the height at which mean drag appears to act (Jackson, 1981). The aerodynamic roughness length ($z_0$) is the height at which wind speed becomes zero in the absence of $z_d$. Theoretically, *LOG* applies in the ISL, where flow is free from individual roughness-element wakes, but still scales with surface length scales only ($z_d$ and $z_0$). However, it has been shown to be applicable both close to roughness elements (Cheng and Castro, 2002) and for a considerable depth of the boundary layer (Macdonald et al., 2000; Castro et al., 2006; Cheng et al., 2007; Kent et al., 2017a).

### 2.2. Adapted power law profile

The power law provides a relation between mean wind speeds ($\overline{U}(z_1)$, $\overline{U}(z_2)$) at two different heights ($z_1$, $z_2$), with a wind shear exponent ($\alpha_{PL}$) describing fetch characteristics:

$$\overline{U}(z_1) = \overline{U}(z_2)\left(\frac{z_1 - z_d}{z_2 - z_d}\right)^{\alpha_{PL}} \tag{2}$$

The exponent, $\alpha_{PL}$ (between 0 and 1), provides a best fit of wind speeds between the two heights and is proportional to the vertical gradient of wind speed with height. Typically, a single value of $\alpha_{PL}$ is used for different surfaces (e.g. Davenport, 1960), which does not allow the exponent to vary with height, stability or directly consider surface roughness (Irwin, 1979; Emeis, 2014). Sedefian's (1980) alteration of the exponent addresses this, and is used here:

$$\alpha_{PL} = \frac{\phi_m\left(\frac{\bar{z}}{L}\right)}{\left[\ln\left(\frac{\bar{z}}{z_0}\right) - \Psi_m\left(\frac{\bar{z}}{L}\right)\right]} \tag{3}$$

The $\bar{z}$ is the geometric mean of the height layer considered, $\bar{z} = [(z_1 - z_d)(z_2 - z_d)]^{0.5}$. $\phi_m$ and $\Psi_m$ are empirical stability functions (which depend upon the Obukhov length, $L$). The formulation in Eq. (3) allows the exponent to increase with surface roughness ($z_0$), decrease with increasing height (i.e. as $z_2$ increases) and incorporate thermal effects upon the vertical wind-speed profile. However, Eq. (3) can only be used where surface layer scaling (i.e. use of $z_d$, $z_0$ and $L$) is appropriate. During the neutral conditions considered here, the $\phi_m$ and $\Psi_m$ functions equate to 1 and 0, respectively.

The mathematical simplicity of the *PL* and limited data requirements are advantageous, given it is observed to provide reasonable estimates of wind speeds between ~30 and 300 m (Counihan, 1975; Segal and Pielke, 1988; Zoumakis, 1993; Cook, 1997; Li et al., 2010), especially during strong wind conditions (Emeis, 2014). It therefore provides the basis for building codes in numerous countries (e.g. China, Japan, Canada, United States) (Ge et al., 2013).

### 2.3. The Deaves and Harris profile

By considering the modulus of mean geostrophic wind speed and its ageostrophic counterpart in the ABL, Deaves and Harris (1978) and Harris and Deaves (1980) describe an adapted similarity theory from that used to derive *LOG*. The 'equilibrium model' ($DH_e$) is based upon an extensive uniform fetch (Deaves and Harris, 1978). However, a 'non-equilibrium model' ($DH_v$) is developed to include upwind fetch variability (Deaves, 1981). Both methods are specifically designed for strong wind conditions, defined by wind speeds greater than 10 m $s^{-1}$ measured at 10 m.

#### 2.3.1. Equilibrium model

For an extensive homogeneous fetch, $DH_e$ is described by (Deaves and Harris, 1978; Harris and Deaves, 1980):

$$h = \frac{1}{\beta}\frac{u_*}{f} \tag{4}$$

$$\overline{U}(z) = \frac{u_*}{\kappa}\left[\begin{array}{l}\ln\left(\frac{z-z_d}{z_0}\right) + 5.75\left(\frac{z-z_d}{h}\right) - 1.88\left(\frac{z-z_d}{h}\right)^2 \\ -1.33\left(\frac{z-z_d}{h}\right)^3 + 0.25\left(\frac{z-z_d}{h}\right)^4\end{array}\right] \tag{5}$$

where $h$ is the gradient height, defined as the height where atmospheric flow is free from surface stresses and becomes geostrophic, $f$ is the Coriolis parameter ($f = 2\Omega sin\Phi$, with $\Omega$ the Earth's angular velocity, $7.29 \times 10^{-5}$ rad $s^{-1}$, and $\Phi$ the latitude) and $\beta = 6$ is an empirically determined constant from experimental profiles over sites with flat, homogeneous terrain. The values preceding the four latter terms in Eq. (5) are also empirical constants, selected to give a parabolic velocity defect law for a substantial portion of the ABL (i.e. the wind-speed gradient increases with increasing height) (Deaves and Harris, 1978). The law provides an empirically based polynomial extension of the vertical range of *LOG* to a height where flow is free from surface stresses (i.e. at the gradient height, $h$). For the lowest ~200 m of the boundary layer, Harris and Deaves (1980) note that the last three terms of Eq. (5) can be neglected, compromising only 1% accuracy. However, all terms are considered during this analysis for completeness.

#### 2.3.2. Non-equilibrium model

The non-equilibrium model ($DH_v$) is based upon 'step-changes' in upwind surface roughness ($z_0$) (Harris and Deaves, 1980; Deaves, 1981). An internal boundary layer (IBL) is assumed to form at each step-change and the wind-speed profile directly above the site of concern (hereafter the "reference" site) can be determined through combining the effective equilibrium profiles for each IBL (according to the model in Section 2.3.1) at the appropriate heights (Harris and Deaves, 1980; Deaves, 1981; ESDU, 2002).

The details given in Harris and Deaves (1980) are complemented with recommendations for use (including calculation sheets) by the Engineering Sciences Data Unit (ESDU) 82026 (ESDU, 2002). However, treating roughness in a 'step-change' framework presents several challenges. Firstly, identification of discrete areas for which upwind aerodynamic roughness parameters should be determined is some-what subjective. Second, the magnitude of roughness change which is sufficient for distinct IBL formation is not well defined and therefore the fetch (i.e. distance upwind) from a reference site where a 'step-change' takes place is difficult to determine. For example, a clear new IBL may fail to develop if there are not sharp changes in surface characteristics (Mahrt, 2000). Thirdly, if an IBL does form, there is uncertainty associated with its growth and therefore expected depth of influence at a reference site (Savelyev and Taylor, 2005).

To overcome such challenges, during this study $DH_v$ is applied using surface observations and a source area footprint model. The source area model is used to determine the probable upwind surface which would be contributing to measurements at pre-defined vertical increments ($z_l$) above the reference site (Fig. 1). Weighted roughness parameters are calculated for each source area (Kent et al., 2017a methodology) and subsequently ESDU (2002) recommendations are used to estimate the

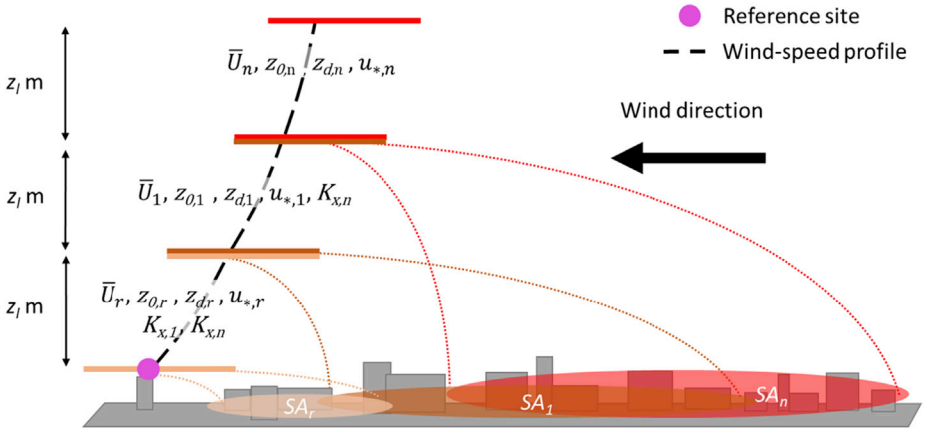


**Fig. 1.** Operation of the Deaves and Harris non-equilibrium wind-speed profile method ($DH_v$) as applied in this work. A source area footprint model is applied at pre-defined vertical increments (height: $z_l$ m) above the reference site. The source area for each respective height ($SA_r$, $SA_1$ and $SA_n$) is used to determine representative roughness parameters ($z_d$ and $z_0$), which are subsequently used to calculate local friction velocities ($u_{*,r}, u_{*,1}, u_{*,n}$). The effective wind-speed profile for each 'layer' (depth $z_l$ m) is then calculated (using Eq. (5)) with the appropriate roughness transition correction ($K_{x,1}$, $K_{x,n}$) (ESDU, 2002). Subscripts are: '$r$' reference (i.e. from the reference site observations), '1' representative of the first calculations performed $z_l$ m above the reference site, and '$n$' for the nth calculation (performed at $n \times z_l$ m above the reference height).

wind-speed profile above the reference site considering multiple changes in upwind roughness (see Fig. 1). Using $DH_v$ with the source area model means that, rather than attempting to identify surface roughness changes which may trigger IBL growth, an integrated representation of the upwind surface is considered. Definition of $z_l$ is some-what arbitrary, but its value should provide a compromise between being large enough for computational efficiency, but small enough to consider significant changes in upwind surface characteristics. The effect of altering $z_l$ is considered later (Section 5.2.2).

### 2.4. The Gryning profile

Using observations above rural, flat and urban surfaces for 10 m wind speeds greater than 3 m $s^{-1}$, Gryning et al. (2007) indicate wind-speed profiles based upon surface layer scaling (i.e. the *LOG* method) are only valid up to a height of approximately 80 m. Above this, Gryning et al. (2007) argue that neutral wind speeds increase at a greater rate than the *LOG* method predicts, as a consequence of the non-linearity of the surface length scale. Therefore, in the Gryning et al. (2007) method (hereafter *GR*) three component length scales are used to represent different parts of the ABL. In addition, the friction velocity is assumed to decrease linearly with height beyond the surface layer. During neutral conditions, the surface length scale ($L_{SL,N}$) is proportional to height, the middle layer length scale ($L_{MBL,N}$) is near constant, and the upper length scale ($L_{UBL,N}$) decreases linearly to the top of the ABL ($L_{UBL,N} = h - (z - z_d)$), therefore:

$$\frac{du}{dz} = \frac{u_*}{\kappa}\left(1 - \frac{z - z_d}{h}\right)\left(\frac{1}{z - z_d} + \frac{1}{L_{MBL,N}} + \frac{1}{h - (z - z_d)}\right) \tag{6}$$

Integrating Eq. (6) between a height, $z$, and where the wind speed falls to zero (at height $z_0$):

$$\overline{U}(z) = \frac{u_*}{\kappa}\left(\ln\left(\frac{z - z_d}{z_0}\right) + \frac{z - z_d}{L_{MBL,N}} - \frac{z - z_d}{h}\left(\frac{z - z_d}{2L_{MBL,N}}\right)\right) \tag{7}$$

Through empirical fits to observed profiles, Gryning et al. (2007) demonstrate $L_{MBL,N}$ can be determined using only surface measurements by:

$$\frac{u_*}{fL_{MBL,N}} = -2\ln\left(\frac{u_*}{fz_0}\right) + 55 \tag{8}$$

To determine $h$, Gryning et al. (2007) recommend using Eq. (4) with a proportionality constant (β) of 10, 9 and 12 for rural (flat and homogeneous), residential and urban areas, respectively. The urban setting of this work means β = 12 is used here.

### 2.5. Vertical extrapolation of the surface wind speed

To extrapolate the neutral wind-speed profile from surface observations using pre-determined aerodynamic roughness parameters ($z_d$ and $z_0$), the *LOG* and *PL* methods only require a reference surface wind speed ($U_{ref}$). The other methods require $u_*$ and $h$, which without observations require an iterative procedure for their determination:

1) $u_*$ is calculated using the surface wind speed ($U_{ref}$) and pre-determined roughness parameters ($z_d$ and $z_0$) by rearranging Eq. (1)
2) $h$ is determined using Eq. (4)
3) The wind-speed profile is extrapolated using Eq. (5) for the $DH_e$ and $DH_v$ methods or Eq. (7) for the *GR* method. Note when using the *GR* method $L_{MBL,N}$ must be calculated prior to this using Eq. (8).
4) A revised $u_*$ is obtained for each respective method from rearranging Eq. (5) or (7), using $U_{ref}$ and $h$
5) Return to step 2) until there is convergence of $u_*$ and $h$

Convergence is rapid, typically requiring only 2–3 iterations for less than 1% variability (which is the convergence criteria used here). From step 1, the procedure is sensitive to the pre-determined $z_d$ and $z_0$.

## 3. Aerodynamic roughness parameters

A pre-requisite to determining the wind-speed profile from surface observations is accurately determining the aerodynamic roughness parameters, $z_d$ and $z_0$. Morphometric methods describe $z_d$ and $z_0$ based upon surface form. The methods can be divided into two classes: (i) those assuming homogenous roughness-element heights, represented by $H_{av}$, and (ii) those considering roughness-element height variability. Collectively the former are termed $RE_{av}$ and the latter $RE_{var}$ (Kent et al., 2017a). For the same study site as used here, Kent et al. (2017a) demonstrate that wind speeds extrapolated using the $RE_{var}$ roughness parameters are most similar to observations. The Kent et al. (2017a) results are developed here by considering additional methods to extrapolate the wind-speed profile, as well as more complex surface cover. Aerodynamic roughness parameters are determined using the Macdonald et al. (1998) (*Mac*) and Kanda et al. (2013) (*Kan*) morphometric methods ($RE_{av}$ and $RE_{var}$ type, respectively). The methods have been developed to include the effects of vegetation (Kent et al., 2017b), which has been shown to improve wind-speed estimation (Kent et al., 2018). However, during this winter (i.e. leaf-off vegetation state), city centre (i.e. building dominated) analysis, vegetation is not expected to critically influence roughness parameters and the extrapolated wind speeds (e.g. Kent et al., 2017b), and is therefore not considered.

The *Mac* method zero-plane displacement ($Mac_{z_d}$) and aerodynamic roughness length ($Mac_{z_0}$) are calculated by:

$$Mac_{z_d} = \left[1 + \alpha_M{}^{-\lambda_p}\left(\lambda_p - 1\right)\right]H_{av} \tag{9}$$

$$Mac_{z_0} = \left(\left(1 - \frac{z_d}{H_{av}}\right)\exp\left[-\left\{0.5\beta_M\frac{C_{Db}}{k^2}\left(1 - \frac{z_d}{H_{av}}\right)\lambda_f\right\}^{-0.5}\right]\right)H_{av} \tag{10}$$

where $C_{Db} = 1.2$ is the drag coefficient for buildings, $\alpha_M = 4.43$ and $\beta_M = 1.0$ are empirical constants for staggered arrays fit to the wind tunnel data of Hall et al. (1996) and $\lambda_p$ and $\lambda_f$ are the plan and frontal area index of roughness elements, respectively.

The *Kan* method directly considers roughness-element height variability through use of the maximum ($H_{\max}$) and the standard deviation ($\sigma_H$) of roughness-element heights and incorporates $Mac_{z_0}$, such that:

$$Kan_{z_d} = \left[c_0X^2 + \left(a_0\,\lambda_p{}^{b_0} - c_0\right)X\right]H_{max}, \quad X = \frac{\sigma_H + H_{av}}{H_{max}} \tag{11}$$

$$Kan_{z_0} = \left(b_1Y^2 + c_1Y + a_1\right)Mac_{z_0}, \quad Y = \frac{\lambda_p\,\sigma_H}{H_{av}} \tag{12}$$

where $0 \le X \le 1$, $0 \le Y$ and $a_0$, $b_0$, $c_0$, $a_1$, $b_1$ and $c_1$, are constants 1.29, 0.36, −0.17, 0.71, 20.21 and −0.77, respectively. The *Kan* method includes the effect of individual tall buildings (i.e. $H_{\max}$) at the 1 km scale (Kanda et al., 2013), but this is expected to become less important with distance from a location. Therefore, when $H_{\max}$ is more than 1 km from the reference site, the height is weighted by the source area.

## 4. Observations

Observations using a Halo Photonics Streamline pulsed Doppler lidar for an eight month period (October 2010–May 2011) are analysed. The instrument was located on King's College London (KCL) Strand campus rooftop, approximately 36 m above ground level (agl) (Fig. 2d, KSSW position). For a detailed description of the site, see Kotthaus and Grimmond (2012, 2014a, 2014b) and Kent et al. (2017a). The lidar operated in Doppler beam swinging (DBS) mode, whereby the measured Doppler

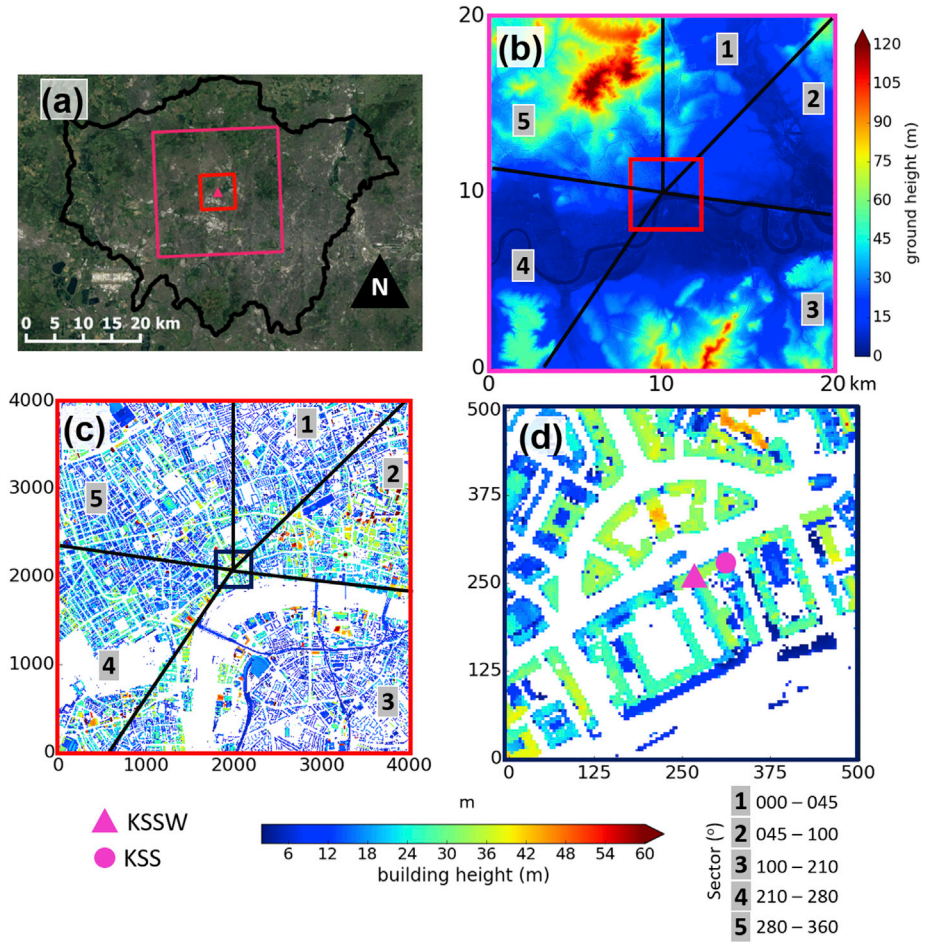


**Fig. 2.** Location of the King's College London (KCL) measurement sites in **(a)** Greater London (black outline), United Kingdom. **(b)** Ground height for the 20 km$^2$ around KCL. Building heights >2 m in the surrounding: **(c)** 4 km$^2$ and **(d)** 500 m$^2$. Sector divisions 1–5 in **(b)** and **(c)** are manually defined based upon upwind surface characteristics (see Section 5.2). Elevation data source: Lindberg and Grimmond (2011).

shift between transmitted and returned pulses provides horizontal wind speed and direction in 30 m vertical gates above the instrument. Beams are transmitted consecutively in three directions (first vertical, then tilted east and north by 15°), with a 21 s scan cycle and the minimum permitted interval between scans is 120 s (Lane et al., 2013). The lidar geometry means only part of the return signal is detected from the lowest three gates, which can therefore not be used. As the lower portion of boundary layer is of interest, only the next three gates are analysed (mid-points 141, 171 and 201 m). Hourly-averages are used to reduce variability in the mean wind speed whilst ensuring stationarity (Lane et al., 2013). To ensure neutral conditions, profiles which have upper quartile wind speeds in all three gates are considered. In addition, only daytime profiles are used (0900–1700 h), to prevent nocturnal boundary layer features (such as jets) influencing results (Mahrt, 1998). The 251 hourly-averaged profiles meeting these criteria, were subdivided by upwind surface characteristics (Section 5.2) into five directional sectors (Fig. 2b and c). Data from a Vaisala CL31 ceilometer, located approximately 3 m south-west of the Doppler lidar, is used to determine the mixing layer height ($H_{ML}$) (Section 5.3).

A CSAT 3 sonic anemometer (Campbell Scientific, USA) mounted on an Aluma T45-H triangular tower measured the 3-dimensional wind velocity and sonic temperature (with a sampling frequency of 10 Hz) approximately 45 m east of the KSSW site (Fig. 2d, KSS site). The anemometer at the KSS site is 48.9 m agl (i.e. 2.5$H_{av}$ in the surrounding 1 km) and 13.3 m above the roof hosting the tower. Minimal distortion of turbulence data indicates measurements are free from local roughness-element wakes and therefore taken within the inertial sublayer (Kotthaus and Grimmond, 2014b; Kent et al., 2017a). For each hourly period, observations at the KSS site are used to apply the Kormann and Meixner (2001) source area footprint model from the lidar position (KSSW) to obtain the *Kan* and *Mac* aerodynamic roughness parameters for wind profile extrapolation (Kent et al., 2017a methodology). For the *LOG*, *PL*, $DH_e$ and *GR* methods only roughness parameters determined from the source area calculations at 49 m height are used. For $DH_v$, the source area model is applied using surface observations at the specified vertical increments ($z_l$) to indicate the probable extent, and associated aerodynamic roughness parameters, of the upwind surface contributing to measurements at each height (e.g. Fig. 1).

## 5. Results

### 5.1. Controlled comparison of the wind-speed profile methods

Comparison of the assessed wind-speed profile methods during similar conditions demonstrates their operation in the lower boundary layer. Assuming a neutrally stratified boundary layer, with a reference wind speed of 10 m s$^{-1}$ ($U_{ref}$) measured at 49 m, the wind-speed profile is extrapolated for 200 m vertically and normalised by $U_{ref}$ (Fig. 3). The aerodynamic roughness parameters ($z_d$ and $z_0$) used during the extrapolation are the typical values reported by the *Mac* and *Kan* methods at the KSSW site. The most obvious difference between these is that $Kan_{z_d}$ is twice $Mac_{z_d}$ (for a more detailed analysis of locally determined $z_d$ and $z_0$ at KCL see Kent et al., 2017a). For the wind profile methods which do not explicitly consider upwind changes in surface roughness (the *PL*, *LOG*,

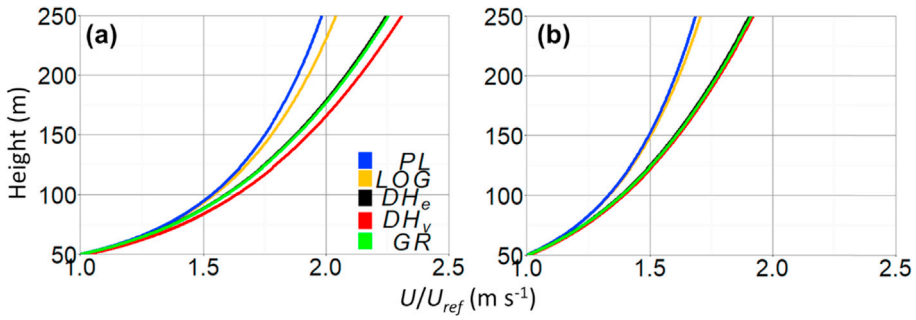


**Fig. 3.** Controlled comparison of the wind-speed profile extrapolated from 50 m using the different methods assessed (Section 2), normalised by a reference wind speed ($U_{ref}$) of 10 m s$^{-1}$. The profiles are extrapolated with roughness parameters characteristic of the study site determined by the **(a)** Kanda et al. (2013) and **(b)** Macdonald et al. (1998) morphometric methods. Profile abbreviations: *PL* – power law; *LOG* – logarithmic wind law; $DH_e$ – Deaves and Harris equilibrium model; $DH_v$ – Deaves and Harris non-equilibrium model; *GR* – Gryning et al. (2007). See text for the values used during the extrapolation.

$DH_e$ and *GR* methods), the roughness parameters used are $z_0 = 2$ m and $z_d = 30$ m (Fig. 3a, representative of $Kan_{z_d}$) or $z_d = 17.5$ m (Fig. 3b, representative of $Mac_{z_d}$). For the $DH_v$ method, $z_l$ is pre-defined as 50 m and three changes in roughness are assumed to influence the profile. The roughness parameters assumed at the bottom of the 50, 100 and 150 m layers are: $z_0 = 2$, 1.5 and 1 m, respectively, with $z_d = 30$, 20 and 10 m (Fig. 3a) or $z_d = 17.5$, 15 and 12.5 m (Fig. 3b). Note that if the surface $z_d$ and $z_0$ are used at each height (representing an extensive homogenous fetch) $DH_v$ collapses to $DH_e$. The Coriolis parameter ($f$) is determined using the latitude of KCL, $\Phi = 51.51°$.

Wind speeds extrapolated using the $DH_e$, $DH_v$ and *GR* methods are similar to each other and all greater than the *LOG* and *PL* methods (Fig. 3). Close to the surface (below 100 m) the methods are dominated by surface-based length scales (i.e. $z_d$ and $z_0$, only) and therefore indicate similar wind speeds. Above this the wind speed gradients of the $DH_e$, $DH_v$ and *GR* methods increase with height as they become influenced by other length scales (e.g. $h$). The *PL* method has similar wind speeds to *LOG*, tending towards lower wind speeds with increasing height.

Wind speeds using the *GR* profile are marginally greater than the $DH_e$ method. The assumed upwind transition from a comparatively smooth to rough surface means the $DH_v$ wind speeds are greater than both the $DH_e$ and *GR* methods. However, the $DH_v$ wind speeds are only a maximum of 2% larger than the $DH_e$ method despite the approximate 50% decrease in upwind $z_d$ and $z_0$ which affects the $DH_v$ profile only.

All wind speeds extrapolated using the *Kan* roughness parameters (Fig. 3a) are greater than using the *Mac* parameters (Fig. 3b). For the *LOG* and *PL* methods, this is because the smaller $z_d$ from the *Mac* method produces less shear. For the other methods the parameters calculated internally to the models ($u_*$ and $h$) take effect. Following rearrangement of Eq. (1), a smaller $z_d$ generates a smaller $u_*$, which in turn gives a smaller $h$ (Eq. (4)). The reduction of $h$ 'squeezes' the wind-speed profile into a smaller depth of ABL and therefore acts to increase the estimated wind speed for any given height. However, this increase is countered by the reduction in $u_*$, which causes a larger decrease in wind speed meaning the overall effect is a reduction of wind speed. In the *GR* method, $u_*$ is also used to calculate the internal parameter $L_{MBL,N}$. A comparatively smaller $z_d$ (and associated reduction in $u_*$) decreases $L_{MBL,N}$, which by the form of Eq. (7) acts to further decrease wind speed. Further attention is given to the internally calculated $u_*$ and $h$ later (Section 5.3).

### 5.2. Upwind surface variability

#### 5.2.1. Upwind surface variability at KCL

The use of just two aerodynamic roughness parameters ($z_d$ and $z_0$) to model the lower ABL wind speed, assumes these two length scales are sufficient to describe the influence of the entire underlying surface at a reference site. The extent to which this assumption is appropriate depends upon upwind surface variability (Deaves, 1981) – the premise of the $DH_v$ method is that surface characteristics further upwind may be more appropriate to describe the wind speed further from the surface (e.g. Fig. 1). The variability of the upwind surface from the KSSW site is assessed by comparing the roughness parameters determined from source areas calculated at 25 m height increments (i.e. $z_l$ is 25 m in Fig. 1), for each hourly period. Note that the roughness parameters will vary with the morphometric method used and therefore so will the modelled source area. For descriptive purposes the *Kan* method is discussed.

As the size of the source area increases with height, both the extent and location of the maximum influence vary. At a height of 200 m, the upwind extent of the source area reaches 5 km, which is (on average) three times larger than that calculated at 100 m (1.8 km upwind), and 30 times that calculated at 49 m (170 m upwind). The source area growth with height means a wide range of building geometries are encountered. This impacts the calculated roughness parameters, such that the variability cannot be generalised in all directions (Fig. 4a and b). The obvious directional differences are used to classify observations into five directional sectors (Table 1, Fig. 2b and c).

In sector 1 (000° – 045° from the KSSW site), as the source area becomes larger with height (e.g. Fig. 1), $H_{av}$, $\lambda_p$ and $\lambda_f$ all decrease gradually. However, taller buildings located approximately 600 m upwind from the KSSW site (Fig. 2c) cause a discontinuous increase in $H_{\max}$ and $\sigma_H$. The dependency of $z_d$ on $H_{\max}$ (Kanda et al., 2013, Eq. (11)) means an initial upwind increase in $z_d$ (from 32 to 36 m) thereafter gradually decreases to 20 m (Fig. 4a). In comparison, $z_0$ gradually decreases from as large as 3 m closer to the site to between 1 and 2 m further afield (Fig. 4b). Sector 5 (280° – 360°) exhibits similar changes in upwind building geometry and roughness parameters to sector 1. However, the topographic variability (upwind vertical ascent of up to 135 m within approximately 6.5 km, Fig. 2b) means the sectors are treated separately.

Sector 2 (045° – 100°) has the greatest height heterogeneity, associated with the tallest buildings in London. High rise buildings, packed in close proximity, generate $\lambda_p$ and $\lambda_f$ of 0.5. In addition, $H_{av}$, $H_{\max}$ and $\sigma_H$ all increase with distance upwind creating an increasingly chaotic surface. Sector 2 is therefore the only direction where surface roughness (both $z_d$ and $z_0$) increases with distance upwind (Fig. 4). Unfortunately, with only six profiles available for this direction, further analysis is impossible.

The presence of the river in sector 3 (100° – 210°) creates a complicated fetch. Sector 3 has the lowest $\lambda_p$ and $\lambda_f$ (0.25) because of the river and comparatively sparse buildings on the far side of the river (Fig. 2c). As $H_{av}$ tends to decrease upwind, so do $z_d$ and $z_0$, except for between 190° – 210° where taller buildings cause an initial increase in $z_d$ and $z_0$ (Fig. 4).

In sector 4 (210° – 280°), $z_d$ decreases from approximately 30 m close to the KSSW site to 25 m further upwind. This is caused by an abrupt reduction in $H_{av}$, which is also responsible for an initial decrease in $z_0$. However, beyond this $H_{av}$ is unchanged and $\lambda_f$ ranges between 0.2 and 0.4, near the peak roughness range (Kent et al., 2017a), therefore $z_0$ becomes larger.

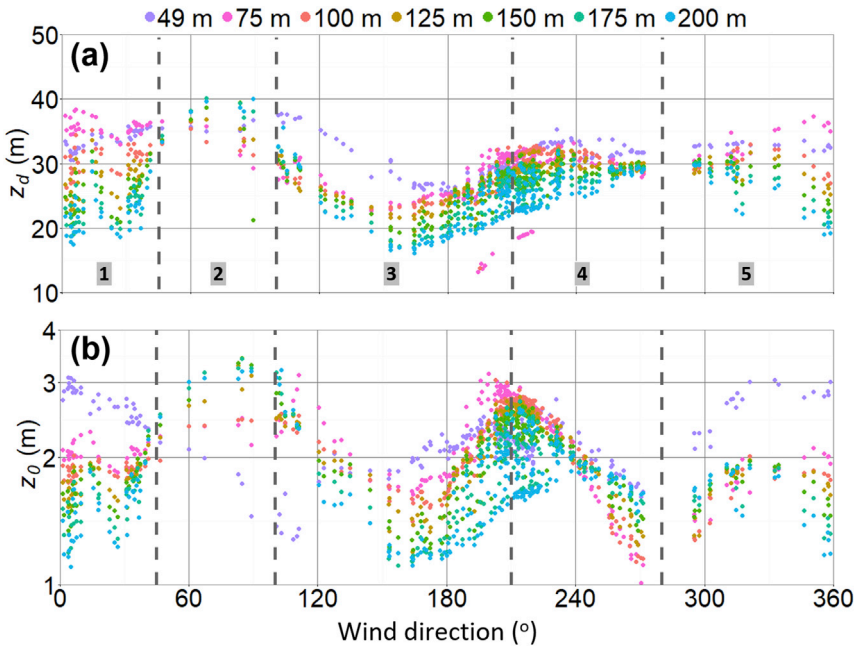


**Fig. 4.** **(a)** Zero-plane displacement ($z_d$) and **(b)** aerodynamic roughness length ($z_0$) (note log axis), determined from source areas calculated in 25 m vertical increments above the KSSW site (colour indicates different heights). For the 251 hourly periods assessed, observations from the KSS site are used with the Kormann and Meixner (2001) footprint model from the KSSW position (Fig. 2) at the heights indicated, with the Kanda et al. (2013) morphometric method to determine $z_d$ and $z_0$ (Kent et al., 2017a methodology). The five directional sectors (dashed lines, 1–5) for analysis (Table 1) are indicated.

A reference-based approach to determine aerodynamic roughness parameters is recommended in ESDU (2002, their Table 13.1), based on a function of $H_{av}$. For cities, ESDU (2002) indicates $z_d$ is between 15 and 25 m and $z_0$ is between 0.5 and 1.5 m. Such reference-based approaches are limited by the subjectivity of application and the inability to model the probable upwind surface contributing to measurements. Roughness parameters determined with the *Kan* method tend to be larger than those indicated in ESDU (2002). This is expected, as the *Kan* method directly accounts for roughness-element height variability (Eqs. (11) and (12)) and the considerable increase in drag exerted by taller roughness elements (Xie et al., 2008; Hagishima et al., 2009; Zaki et al., 2011; Mohammad et al., 2015). Whereas, the *Mac* parameters are closer to the ESDU (2002) values as *Mac* incorporates $H_{av}$ only (Eqs. (9) and (10)).

### 5.2.2. *Influence of the upwind surface variability on the wind-speed profile*

The $DH_v$ method is a development of $DH_e$, allowing $z_d$ and $z_0$ to vary as a function of height in the wind-speed profile. Comparison of the $DH_e$ and $DH_v$ profiles therefore demonstrates the implications of considering upwind roughness in this work. The mean of extrapolated wind-speed profiles in sector 1 reveals wind speeds estimated by the $DH_v$ method are greater than the $DH_e$ method throughout the profile, due to the reduction in upwind roughness (Fig. 5). The maximum wind speed difference is largest (15%), as expected, at greater heights, where roughness parameters have maximum difference from those determined at the surface (Fig. 4).

**Table 1**
Directional sectors used for analysis with the number of hourly profiles. Upwind surface characteristics around the KSSW site (see Fig. 2b and c and Fig. 4) are used for the classification, based on the wind direction observed in the first usable Doppler lidar gate (mid-point = 141 m).

| Sector | 1 | 2 | 3 | 4 | 5 |
|---|---|---|---|---|---|
| Angle from KSSW | 000°–045° | 045°–100° | 100°–210° | 210°–280° | 280°–360° |
| Number of profiles | 36 | 6 | 91 | 98 | 20 |

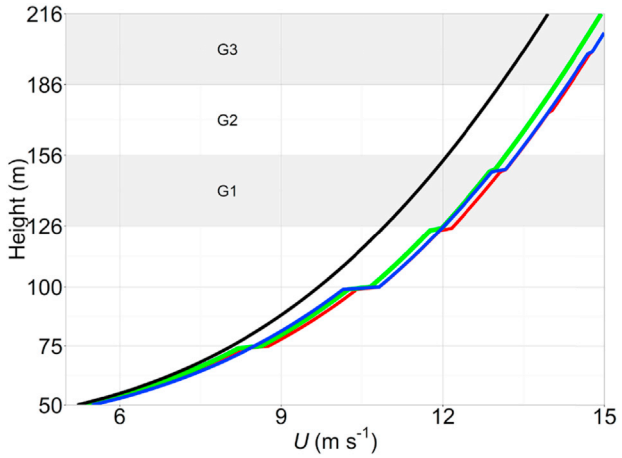


**Fig. 5.** Mean of extrapolated wind-speed profiles in sector 1 ($n$ = 36) using the $DH_e$ method (black line) and $DH_v$ method with height increment ($z_l$) = 50 m (blue line) and $z_l$ = 25 m (red line). For the $DH_v$ method the extent of the upwind surface considered is dictated by the source area calculated at 200 m, which is altered to 150 m for comparison (green line). The 30 m wind gates used from lidar observations during this work are shaded G1 – G3 (G1 = 126–156 m, mid-point = 141 m).

When using the $DH_v$ method, the recalculation of the wind-speed profile at each $z_l$ height increment results in a corrective shift (Fig. 5) which is not expected empirically. The size of each shift depends upon the change in roughness of the upwind surface, as well as the height increment ($z_l$) at which re-calculations are performed. For example, the magnitude of the correction is least where there is less variation in roughness parameters towards the top of the profile (Fig. 4). In addition, comparison between wind profiles using $z_l$ = 25 m and 50 m (red and blue line in Fig. 5, respectively) demonstrates how less frequent recalculation of the wind profile results in larger corrective shift, as the difference between $z_d$ and $z_0$ of each upwind surface increases. Reducing $z_l$ from 50 m to 25 m creates a maximum difference of wind speed at any given height of just 3%. Further reduction of $z_l$ results in an even smaller

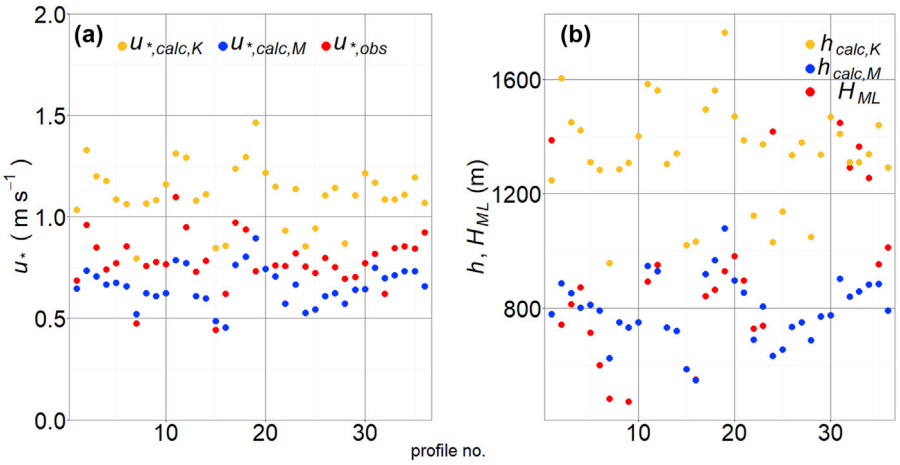


**Fig. 6.** For each hourly period assessed in sector 1 (000° – 045° wind direction from the KSSW site): **(a)** friction velocity calculated internally to the $DH_e$ model ($u_{*,calc}$) and from observations at the KSS site ($u_{*,obs}$); and, **(b)** gradient height ($h$) determined internally to the $DH_e$ model and the mixing layer height determined from observations ($H_{ML,}$ average of two observation methods, see text). Subscripts *K* and *M* refer to use of the Kanda et al. (2013) and Macdonald et al. (1998) aerodynamic roughness parameters during calculations, respectively.

difference and considering the extra computational requirements, $z_l = 25$ m is deemed sufficient.

Definition of the pertinent fetch for a reference site (i.e. upwind distance of surfaces influencing the profile aloft) is problematic and not addressed well in building codes (e.g. ESDU, 2002; Abdi and Bitsuamlak, 2014). Earlier work demonstrates that the fetch may be modelled through consideration of flow parameters (Elliott, 1958) or upwind roughness (Miyake, 1965; Wieringa, 1993) and that surfaces up to 200 km upwind from a reference site will still have some influence upon the wind-speed profile (Cook, 1985). However, recent work indicates only characteristics much closer to a site are of significance for a rough surface (Tamura et al., 2001, Zhang and Zhang 2001, AS/NZS (1170.2) 2002, Wang and Stathopoulos 2007). This has been associated with more rapid IBL development (Tamura et al., 2001) and contrasts with wind tunnel experiments indicating IBL growth may be slower than classical results suggest (Cheng and Castro, 2002).

The unclear definition of the pertinent fetch means that in this work, the maximum upwind extent of the surface considered is limited by the maximum height where source area calculations are performed, which is 200 m (red line, Fig. 5). Reducing this value to 150 m (green line, Fig. 5) causes a variation in wind speed above 150 m because of the disregard for upwind roughness contributing to the profile above this height. However, wind speeds below 150 m remain similar. These results exemplify that in the current application of $DH_v$, considering roughness contributing to the profile beyond a height of interest does not obviously influence wind speeds below that height. Given the focus of this work on the lower ABL, considering a maximum height of 200 m is therefore deemed sufficient.

### 5.3. Internal parameters used in the wind-speed profile methods

When estimating the wind-speed profile, $u_*$ and $h$ are calculated internally by the respective wind profile models (Section 2.5). The gradient height ($h$) determined by the models as the height where ABL flow becomes free from surface stresses, does not necessarily coincide with the mixing layer height ($H_{ML}$) determined using observations and various methods (Emeis et al., 2008). Comparison of the internally calculated parameters using the $DH_e$ method ($u_{*,calc}$, $h_{calc}$) with those obtained from meteorological instrumentation at KCL ($u_{*,obs}$, $H_{ML}$) tests this argument. For each hourly period, $u_{*,calc}$ and $h_{calc}$ are determined using the method outlined in Section 2.5, with the observed wind speed and roughness parameters determined from 49 m. The $u_{*,obs}$ is calculated using high frequency observations (Leclerc and Foken, 2014): $u_{*,obs} = [(\overline{u'w'})^2 + (\overline{v'w'})^2]^{1/4}$. Two independent methods are used to obtain $H_{ML}$ using the Doppler lidar and automated lidar/ceilometer (using the methods described in Barlow et al., 2015; Kotthaus and Grimmond, 2017, respectively) and their average is used as an indication of $H_{ML}$.

For the 36 periods in sector 1 (000° – 045° from KSSW), $u_{*,obs}$ varies between 0.4 and 1.0 m s$^{-1}$ (Fig. 6a). These are typically expected magnitudes for an urban area (e.g. Roth, 2000). Similarly, $H_{ML}$ ranges between typically expected winter UBL heights (e.g. Seidel et al., 2010) with an average depth of 930 m (Fig. 6b). If the parameters are calculated internally to the wind-speed profile methods, they are sensitive to the morphometric method used and most similar to the observed values when using the *Mac* roughness parameters (Fig. 6, $u_{*,calc,M}$ and $h_{calc,M}$). Using the *Kan* roughness parameters, the friction velocity is on average 40% larger and $h$ can be up to twice as large as $H_{ML}$.

To assess the suitability of the parameters, the mean of extrapolated wind speeds in sector 1 are compared using the $DH_e$ method with: (i) internally calculated parameters ($u_{*,calc}$ and $h_{calc}$); and (ii) observed $u_{*,obs}$

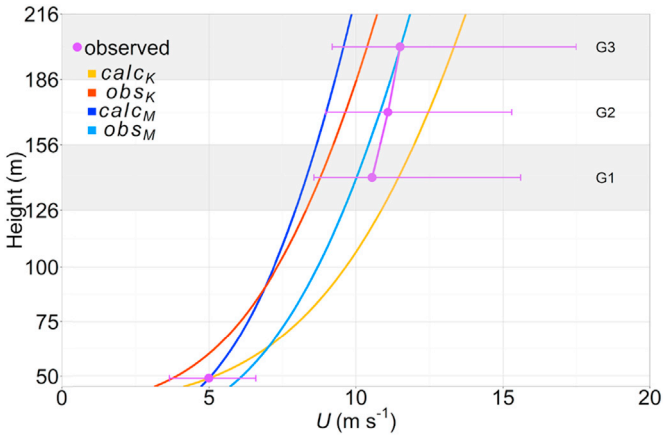


**Fig. 7.** Mean wind-speed profiles extrapolated using the Deaves and Harris equilibrium model ($DH_e$) for all hourly periods assessed in sector 1 ($n$ = 36). The profiles are extrapolated using parameters calculated internally to the model (*calc*) and from observations (*obs*). Subscripts *K* and *M* indicate use of Kanda et al. (2013) and Macdonald et al. (1998) aerodynamic roughness parameters, respectively. The mean observed wind speed at 49 m by a sonic anemometer and 30 m wind gates of the lidar are shown with whiskers to indicate the minimum and maximum observed wind speeds. The 30-m lidar gates are shaded G1 – G3, with mid-points: G1 = 141 m, G2 = 171 m and G3 = 201 m.

and $H_{ML}$ (Fig. 7). Using the internally calculated parameters, the modelled wind speeds at the extrapolation height (49 m) are equal to the observed wind speed, by definition. Above this, following Section 5.1 wind-speed estimations are larger using the *Kan* method. When $u_{*,obs}$ and $H_{ML}$ are used, the estimated wind speeds are not constrained to a wind-speed at any height. Additionally, wind-speed estimates throughout the profile are larger when using the *Mac* roughness parameters because the bias from the internally calculated $u_*$ and $h$ no longer takes effect. The variation from observed wind speeds is largest near the surface (at 49 m) with an average difference of up to 30%. However, estimations are more similar to observations aloft, especially when using the *Mac* roughness parameters. The $u_{*,obs}$ and $H_{ML}$ are rarely available during routine wind-speed profile estimations, therefore the internally calculated parameters are used during this work. However, the comparison indicates it is not unreasonable to use an observed $u_*$ and $H_{ML}$ when using the different profile methods.

### 5.4. Variability of observed wind speeds

Wind speeds observed in the UBL are, amongst other controls, a function of synoptic-scale forcing, topographical conditions, anthropogenic activity, and surface characteristics (e.g. Britter and Hanna, 2003; Fernando, 2010; Barlow, 2014). Without additional measurements to those at KCL it is difficult to identify the impact of each upon the observed wind profile, however, comparison of wind speeds throughout the profile provides useful insight.

The lowest mean wind speeds observed throughout the profile are to the north and north-west (sectors 1 and 5), which are between 4.5 m s$^{-1}$ and 5 m s$^{-1}$ at the surface and 10.5 m s$^{-1}$ and 11.5 m s$^{-1}$ aloft (Fig. 8a).

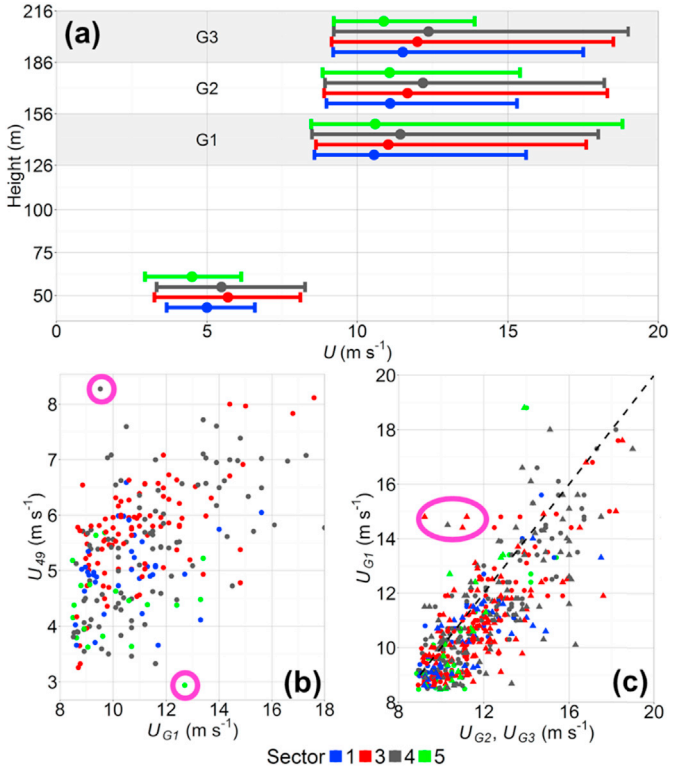


**Fig. 8.** For all observations ($n$ = 245): **(a)** average (points) and minimum/maximum (whiskers) observed wind speed at 49 m and 30 m gates of the Doppler lidar (shaded G1 – G3). Wind speed observed at: **(b)** 49 m ($U_{49}$) and the first gate of the lidar ($U_{G1}$), and **(c)** $U_{G1}$ and the second ($U_{G2}$, circles) and third ($U_{G3}$, triangles) gates of the lidar, with a 1:1 relation (dashed line). Points circled in magenta are referred to in text. Data are selected through the filtering process outlined in Section 4 and coloured by wind direction (see Table 1 for sector definitions).

The highest mean wind speeds occur in southerly directions (sectors 3 and 4). The directional variability of wind speeds is predominantly dictated by synoptic-scale forcing, with frequent frontal passage across the UK (typically from west to east) resulting in stronger winds from the southwest and less frequent, lower wind speeds from the northeast. However, it is also possible that the gradual reduction in upwind roughness to the north of the sites may be contributing to the lower observed wind speeds (e.g. Deaves, 1981) (Fig. 4). The linear MS-micro/3 wind flow model (Walmsley et al., 1986, 1990) indicates that the surrounding topography (including the gently sloping topography to the north) does not obviously influence wind speed at the site.

The larger shear stress experienced closer to the surface is responsible for the observed wind speed at 49 m (approximately 2.5 times the canopy height) consistently being approximately half of that observed 200 m above the canopy (Fig. 8a). However, wind speeds do not always behave as expected throughout the profile. This is exemplified by two extreme cases (circled in Fig. 8b): one where a wind speed of approximately 9 m s$^{-1}$ is observed both at 49 m ($U_{49}$) and the first gate of the lidar ($U_{G1}$); and another where $U_{49}$ is just 3 m s$^{-1}$ at the same time $U_{G1}$ is 12.5 m s$^{-1}$. A likely source of this variability is that on occasion, the surface measurements and those aloft are responding to different flow fields as a consequence of longitudinal and transverse roughness heterogeneity upwind. Measurements closer to the surface may be responding to local obstacles, whilst flow aloft is a function of the integrated or blended surface (Grimmond and Oke, 1999; Roth, 2000; Grimmond et al., 2004; Barlow et al., 2008; Barlow, 2014). This is supported by the better agreement of observed wind speeds aloft (between 126 and 216 m) (Fig. 8c), where the effects of local surface roughness variability are less pronounced. However, deviations from the idealised profiles still occur, such as the grouping of observations where wind speed decreases with height (circled in Fig. 8c). This demonstrates the uncertainties arising when using idealised wind profile relations to estimate the wind-speed profile.

### 5.5. Comparison of observed and estimated wind-speed profiles

The directional variability and range of upwind surface roughness, wind speed, observational frequency and topographical variability, means that a collective analysis of wind profiles results in a bias towards more frequently observed wind directions or extremes. Hence a comparison of the observed ($U_{obs}$) and extrapolated wind speed by each of the wind profile methods ($U_{ext}$) is performed for each directional sector. For each hourly period, $U_{ext}$ is calculated at 1 m height intervals and averaged over 30 m gates to correspond to the vertical resolution of the lidar. The difference ($U_{diff}$) between $U_{ext}$ and $U_{obs}$ for each 30 m gate is summarised in Fig. 9.

For all wind profile methods, the aloft wind-speed estimates are consistently most similar to $U_{obs}$ (i.e. $U_{diff}$ is closest to 0 m s$^{-1}$ in Fig. 9a–d) when the *Kan* method parameters are used. Whereas, using the *Mac* roughness parameters means wind speeds are underestimated (Fig. 9e–h). This is most obvious for the *PL* and *LOG* methods because of their least steep gradients. Both predict similar wind speeds, underestimating wind speeds in over 95% of cases with a median of between 2.5 m s$^{-1}$ and 4.5 m s$^{-1}$ (Fig. 9e–h). In more extreme cases, the underestimation can be up to 9 m s$^{-1}$ (Fig. 9h), corresponding to almost 90% of the mean observed wind speed at the same height. The greater wind speeds extrapolated using the $DH_e$, $DH_v$ and *GR* methods better resemble observations, however the wind speed is still underestimated on over 80% of occasions, with median underestimation ranging between 1 and 3 m s$^{-1}$. Wind speeds are most obviously underestimated in sector 5 (Fig. 9h), as the models have underestimated the large shear between surface and upper winds for this direction (Fig. 8a, b).

The greater extrapolated wind speeds with the *Kan* roughness parameters are more similar to $U_{obs}$, with occasional overestimation, especially further from the surface (Fig. 9a–d). The reduced shear of the *PL* and *LOG* profiles cause wind speeds to be underestimated

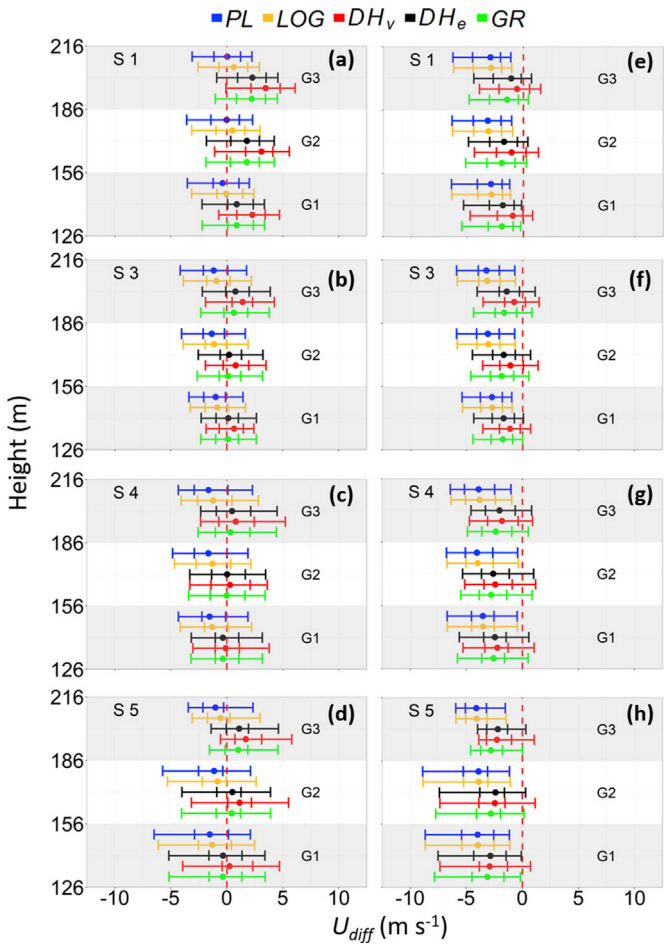


**Fig. 9.** Distribution of hourly wind speed differences ($U_{diff}$) between observed ($U_{obs}$) and extrapolated ($U_{ext}$) wind speeds at heights corresponding to 30 m lidar gates (Gates shaded G1 – G3) ($U_{diff} = U_{ext} - U_{obs}$). Points are the median and whiskers are the 5th, 25th, 75th and 95th percentiles. The analysis is stratified into directional sectors, labelled S1, S3, S4, S5 (see Table 1 for directions). Differences shown are using **(a–d)** Kanda et al. (2013) and **(e–h)** Macdonald et al. (1998) roughness parameters. Profile abbreviations: *PL* – power law; *LOG* – logarithmic wind law; $DH_e$ – Deaves and Harris equilibrium model, $DH_v$ – Deaves and Harris non-equilibrium model; *GR* – Gryning et al. (2007).

approximately 75% of the time (medians between 0.5 and 2 m $s^{-1}$). However, as the wind shear is smallest in sector 1, the *PL* and *LOG* profiles best resemble $U_{obs}$, and the other methods overestimate (Fig. 9a). Despite the *LOG* profile being consistently reported to be appropriate only close to the surface (e.g. Roth, 2000), studies have shown its applicability to up to 50% of the boundary layer depth (Macdonald et al., 2000; Castro et al., 2006; Cheng et al., 2007). Therefore, the similarity of the *LOG* method to $U_{obs}$ at 200 m above the canopy is not unreasonable.

Using the *Kan* parameters from the remaining wind directions (sectors 3, 4 and 5), the greater wind speeds of $DH_e$, $DH_v$ and *GR* best resemble observations (Fig. 9b–d). Of these, the $DH_e$ and *GR* profiles are most consistently similar to $U_{obs}$, as the larger shear of the $DH_v$ profile causes slight overestimation with height (i.e. second and third lidar gates). This is more obvious in sectors 1 and 5, where a combination of the lowest synoptically-driven winds and decreasing upwind roughness causes the smallest observed wind shear (Fig. 8). The increased wind shear indicated by the $DH_v$ profile is a response to the reduction in upwind roughness (Fig. 4). Although uncertainties arise from calculating roughness parameters using the source area model and morphometric methods, the $DH_v$ method overestimation is consistent with Drew et al. (2013), indicating $DH_v$ may be oversensitive to reductions in upwind roughness.

Across all comparisons, $|U_{diff}|$ is largest when the range of observed wind speeds throughout the profile is greatest and most variable. This is most obvious in sector 5, where the observed wind speed variability is not well correlated throughout the profile (Fig. 8), producing the largest range of $U_{diff}$ (consistently ±5 m $s^{-1}$ from the median), which is up to 50% of the mean wind speed. The range of observed wind speeds increases with height in sectors 1, 3 and 4 and therefore so does the range of $U_{diff}$. Despite the increasing mean wind speed with height, the differences relative to the mean wind speed also slightly increase in these directions. For example, using the *Kan* method roughness parameters maximum differences range from between 24%–45% for the lowest lidar gate, to between 35%–53% for the upper gate.

Calculation of the Monin-Obukhov stability parameter ($z'/L$, where $z' = z - z_d$) indicates that the variability of estimates from observations is not likely to be associated with stability effects. Using observations from the KSS site and the $z_d$ value from the *Kan* method (which provides the most accurate wind-speed estimations), over 97% of the hourly observations assessed have $|z'/L| \leq 0.1$, a range which corresponds to near neutral atmospheric stability (Roth, 2000). The remaining values are within $|z'/L| \leq 0.2$ and eliminating these periods from the analysis does not obviously improve wind-speed estimations.

A more likely cause of the variability is that each wind-speed profile method has its own inherent assumptions and is designed or derived based upon a specific set of boundary conditions. Inherent assumptions of the *LOG*, *PL*, *GR* and $DH_e$ methods are that there is an extensive homogeneous fetch, which is rare in urban areas. In addition, the $DH_e$ and $DH_v$ methods are developed for wind speeds greater than 10 m $s^{-1}$ measured at 10 m in rural, open surface conditions (Harris and Deaves, 1980) and the *GR* method is developed using wind speeds greater than 3 m $s^{-1}$ at 10 m (Gryning et al., 2007). A 10 m measurement at the current study site would inappropriately be within the canopy (and not the constant-flux layer), therefore the more suitable height of 2.5 times the canopy height is used. In addition, the wind speeds observed during the analysis were on average only half of the minimum wind speeds used to develop the $DH_e$ and $DH_v$ methods (Fig. 8). Variability is expected when using the wind profile methods outside the conditions they were developed for, however, assessment of their performance is valuable, especially for heterogeneous urban surfaces, which have the greatest potential to breach the assumptions inherent to each method.

## 6. Conclusions

Using wind speeds observed at approximately 2.5 times the canopy height in a central business district (London, UK), wind-speed profiles were extrapolated to 200 m above the canopy using five different methods: the logarithmic wind law (Blackadar and Tennekes, 1968) (*LOG*); the Deaves and Harris equilibrium ($DH_e$) and non-equilibrium ($DH_v$) models (Deaves and Harris, 1978; Harris and Deaves, 1980); an adaptation of the power law (Sedefian, 1980) (*PL*) and the Gryning et al. (2007) (*GR*) profile. The profiles require aerodynamic roughness parameters ($z_d$ and $z_0$), which were determined using the Kent et al. (2017a) iterative methodology with the Kanda et al. (2013) (*Kan*) and Macdonald et al. (1998) (*Mac*) morphometric methods. The extrapolated wind speeds were compared to wind speeds observed with Doppler lidar during strong wind conditions. Based upon surface layer scaling, all of the observations have (or are very close to) neutral atmospheric stability. Directional variations in the upwind surface characteristics warranted separation into consistent sectors. The most appropriate wind-speed profile method depended upon the morphometric method used, the observed wind speed and upwind surface characteristics.

When using the $DH_e$, $DH_v$ and *GR* profiles, the friction velocity and gradient height are required, which are calculated internally to the methods (using their respective equations). Use of the observed friction velocity (at approximately 2.5 times the canopy height) and mixing layer height determined from remote sensing meteorological instruments is demonstrated to also lead to reasonable wind-speed estimates. However,

these observed values are typically unavailable during routine wind-speed estimation, therefore the internally calculated parameters are used during this work.

Irrespective of the wind-speed profile method used, the estimated wind speed is sensitive to the aerodynamic roughness parameters $z_d$ and $z_0$. For all of the wind-speed profile methods assessed, the greater wind speeds estimated when using the *Kan* aerodynamic roughness parameters most resembled observed wind speeds, whereas the *Mac* parameters resulted in wind-speed underestimation. Direct consideration of roughness-element height variability (as the *Kan* method does) appears to be critical to the aerodynamic roughness parameters and hence accurately estimating the wind-speed profile. Assuming the *Kan* roughness parameters are appropriate, the central London comparison indicated that for most conditions the $DH_e$ and *GR* methods were the most suitable to extrapolate the wind speed. However, wind-speed estimations with the $DH_v$ profile are similar and closer to observations than the *PL* and *LOG* methods, which tend to underestimate wind speeds. An exception was in directions with lower wind speeds and gradual reduction in upwind roughness, where the resulting reduced wind shear meant that the *PL* and *LOG* profiles were more appropriate.

Selecting the most appropriate combination of morphometric and wind-speed profile methods meant wind speeds up to 200 m above could be consistently estimated with a median difference of 0 m $s^{-1}$ from observations. However, variability of ±5 m $s^{-1}$ (approximately 50% of the mean wind speed) for hourly wind estimates was unavoidable, which was attributed to using the profile methods outside of the conditions they were developed for, as well as the actual observed variability of wind speed throughout the vertical profile. The observed variability was possibly caused by the longitudinal and transverse surface heterogeneity upwind resulting in airflow throughout the profile being in equilibrium with different upwind surfaces. However, using the $DH_v$ method which accounts for upwind roughness variability did not notably improve wind-speed estimation.

Few observations from directions with pronounced roughness-element height heterogeneity meant these conditions were not addressed. Consequently, the results pertain to a relatively homogeneous European city centre. There is a requirement for comparisons between extrapolated and observed wind speeds above other urban areas, to inform the appropriateness of both the morphometric and wind-speed profile methods assessed during this work and to inform current engineering standards.

## Acknowledgements

This work is funded by a NERC CASE studentship in partnership with Risk Management Solutions (NE/L00853X/1) and the Newton Fund/Met Office CSSP China to SG is gratefully acknowledged. We thank Christos Halios for the provision of the Doppler lidar observations and Simone Kotthaus for provision of the ceilometer derived mixing layer heights, as well as processing of the data collected from the tower mounted instruments. We also thank all of those who maintain the daily operations, collection and processing of data for the London Urban Meteorological Observatory network. We are grateful to Omduth Coceal and Sylvia Bohnenstengel for discussions regarding the analysis.

## References

Abdi, D., Bitsuamlak, G.T., 2014. Numerical evaluation of the effect of multiple roughness changes. Wind Struct. 19, 585–601.
Al-Jiboori, M.H., Fei, H., 2005. Surface roughness around a 325-m meteorological tower and its effect on urban turbulence. Adv. Atmos. Sci. 22, 595–605.
Allwine, K.J., Shinn, J.H., Streit, G.E., Clawson, K.L., Brown, M., 2002. Overview of URBAN 2000: a multiscale field study of dispersion through an urban environment. Bull. Amer Meteor Soc. 83, 521–536.
AS/NZS, 2002. Joint Technical Committee Australian/New Zealand Standard, Structural Design Actions. Part 2: wind actions. Standards Australia International Ltd and Wellington: Standards New Zealand, Sydney.
Barlow, J.F., 2014. Progress in observing and modelling the urban boundary layer. Urban Clim. 10, 216–240.
Barlow, J.F., Rooney, G., von Hünerbein, S., Bradley, S., 2008. Relating urban surface-layer structure to upwind terrain for the Salford Experiment (Salfex). Boundary-Layer Meteorol. 127, 173–191.
Barlow, J.F., Dunbar, T., Nemitz, E., Wood, C.R., Gallagher, M., Davies, F., O'Connor, E., Harrison, R., 2011. Boundary layer dynamics over London, UK, as observed using Doppler lidar during REPARTEE-II. Atmos. Chem. Phys. 11, 2111–2125.
Barlow, J.F., Halios, C.H., Lane, S., Wood, C.R., 2015. Observations of urban boundary layer structure during a strong urban heat island event. Environ. Fluid Mech. 15, 373–398.
Belcher, S.E., 2005. Mixing and transport in urban areas. Philos. Trans. A Math. Phys. Eng. Sci. 363, 2947–2968.
Blackadar, A.K., Tennekes, H., 1968. Asymptotic similarity in neutral barotropic planetary boundary layers. J. Atmos. Sci. 25, 1015–1020.
Britter, R., Hanna, S., 2003. Flow and dispersion in urban areas. Annu. Rev. Fluid Mech. 35, 469–496.
Castro, I.P., Cheng, H., Reynolds, R., 2006. Turbulence over urban-type roughness: deductions from wind-tunnel measurements. Boundary-Layer Meteorol. 118, 109–131.
Cheng, H., Castro, I.P., 2002. Near wall flow over urban-like roughness. Boundary-Layer Meteorol. 104, 229–259.
Cheng, H., Hayden, P., Robins, A., Castro, I., 2007. Flow over cube arrays of different packing densities. J. Wind Eng. Ind. Aerodyn. 95, 715–740.
Cook, N.J., 1985. The Designer's Guide to Wind Loading of Building Structures, Part I: Background, Damage Survey, Wind Data and Structure Classification. Building Research Establishment Report. Butterworths, London, p. 371.
Cook, N.J., 1997. The Deaves and Harris ABL model applied to heterogeneous terrain. J. Wind Eng. Ind. Aerodyn. 66, 197–214.
Counihan, J., 1975. Adiabatic atmospheric boundary layers: a review and analysis of data from the period 1880–1972. Atmos. Environ. 9, 871–905.
Davenport, A., 1960. Wind Loads on Structures. Technical Paper No. 88. Division of Building Research, National Research Council of Canada, Ottawa, Canada.
Deaves, D., 1981. Computations of wind flow over changes in surface roughness. J. Wind Eng. Ind. Aerodyn. 7, 65–94.
Deaves, D., Harris, R., 1978. A Mathematical Model of the Structure of Strong Winds. Construction Industry Research and Information Association Report number 76, London, England.
Drew, D.R., Barlow, J.F., Lane, S.E., 2013. Observations of wind speed profiles over Greater London, UK, using a Doppler lidar. J. Wind Eng. Ind. Aerodyn. 121, 98–105.
Elliott, W.P., 1958. The growth of the atmospheric internal boundary layer. Eos, Trans. Am. Geophys. Union 39, 1048–1054.
Emeis, S., 2004. Vertical wind profiles over an urban area. Meteorol. Z. 13, 353–359.
Emeis, S., 2014. Current issues in wind energy meteorology. Meteorol. Appl. 21, 803–819.
Emeis, S., Baumann-Stanzer, K., Piringer, M., Kallistratova, M., Kouznetsov, R., Yushkov, V., 2007. Wind and turbulence in the urban boundary layer–analysis from acoustic remote sensing data and fit to analytical relations. Meteorol. Z. 16, 393–406.
Emeis, S., Schäfer, K., Münkel, C., 2008. Surface-based remote sensing of the mixing-layer height–a review. Meteorol. Z. 17, 621–630.
Emejeamara, F., Tomlin, A., Millward-Hopkins, J., 2015. Urban wind: characterisation of useful gust and energy capture. Renew. Energy 81, 162–172.
ESDU (Engineering Sciences Data Unit), 2002. Data Item 82026: Strong Winds in the Atmospheric Boundary Layer, Part 1: Hourly-mean Wind Speeds, vol. 55.
Etling, D., 2002. Theoretische Meteorologie Eine Einführung. Springer-Verlag, Berlin, Heidelberg, New York, p. 354.
Fernando, H., 2010. Fluid dynamics of urban atmospheres in complex terrain. Annu. Rev. Fluid Mech. 42, 365–389.
Frehlich, R., Meillier, Y., Jensen, M.L., Balsley, B., Sharman, R., 2006. Measurements of boundary layer profiles in an urban environment. J. Appl. Meteorol. Climatol. 45, 821–837.
Garratt, J., 1992. The Atmospheric Boundary Layer. Cambridge Atmospheric and Space Science Series. Cambridge University Press, Cambridge, p. 444.
Ge, Y., Cao, S., Jin, X., 2013. Comparison and harmonization of building wind loading codes among the Asia-Pacific Economies. Front. Struct. Civ. Eng. 7, 402–410.
Grimmond, C.S.B., Oke, T.R., 1999. Aerodynamic properties of urban areas derived from analysis of surface form. J. Appl. Meteorol. 38, 1262–1292.
Grimmond, C.S.B., Salmond, J., Oke, T.R., Offerle, B., Lemonsu, A., 2004. Flux and turbulence measurements at a densely built-up site in Marseille: heat, mass (water and carbon dioxide), and momentum. J. Geophs Res. Atmos. 109, D24101.
Gryning, S., Batchvarova, E., Brümmer, B., Jørgensen, H., Larsen, S., 2007. On the extension of the wind profile over homogeneous terrain beyond the surface boundary layer. Boundary-Layer Meteorol. 124, 251–268.
Gryning, S., Batchvarova, E., Quante, M., Matthias, V., 2011. Evaluation of vertical profiles in mesoscale meteorological models based on observations for the COST728 study of winter 2003 PM episodes in Europe. In: Steyn, D.G., Castelli, S.T. (Eds.), Air Pollution Modeling and its Application XXI. Springer, Dordrecht, pp. 499–503.
Hagishima, A., Tanimoto, J., Nagayama, K., Meno, S., 2009. Aerodynamic parameters of regular arrays of rectangular blocks with various geometries. Boundary-Layer Meteorol. 132, 315–337.
Hall, D., Macdonald, J.R., Walker, S., Spanton, A.M., 1996. Measurements of Dispersion within Simulated Urban Arrays—a Small Scale Wind Tunnel Study. BRE Client Report, CR178/96.

Harris, R.I., Deaves, D.M., 1980. The structure of strong winds, paper no. 4. In: Proceedings of the CIRIA Conference, London, 12–13 November 1980, Construction Industry Research and Information Association, 6 Storey's Gate, London SW1P 3AU.
Högström, U., 1996. Review of some basic characteristics of the atmospheric surface layer. Boundary-Layer Meteorol. 78, 215–246.
Irwin, J.S., 1979. A theoretical variation of the wind profile power-law exponent as a function of surface roughness and stability. Atmos. Environ. 13, 191–194.
Ishugah, T., Li, Y., Wang, R., Kiplagat, J., 2014. Advances in wind energy resource exploitation in urban environment: a review. Renew. Sustain. Energy Rev. 37, 613–626.
Jackson, P., 1981. On the displacement height in the logarithmic velocity profile. J. Fluid Mech. 111, 15–25.
Kanda, M., Inagaki, A., Miyamoto, T., Gryschka, M., Raasch, S., 2013. A new aerodynamic parametrization for real urban surfaces. Boundary-Layer Meteorol. 148, 357–377.
Kent, C.W., Grimmond, C.S.B., Barlow, J., Gatey, D., Kotthaus, S., Lindberg, F., Halios, C.H., 2017a. Evaluation of urban local-scale aerodynamic parameters: implications for the vertical profile of wind speed and for source areas. Boundary-Layer Meteorol. 164, 183–213.
Kent, C.W., Grimmond, C.S.B., Gatey, D., 2017b. Aerodynamic roughness parameters in cities: inclusion of vegetation. J. Wind Eng. Ind. Aerodyn. 169, 168–176.
Kent, C.W., Lee, K., Ward, H.C., Hong, J.W., Hong, J., Gatey, D., Grimmond, C.S.B., 2018. Aerodynamic Roughness Variation with Vegetation: Analysis in a Suburban Neighbourhood and a City Park. https://doi.org/10.1007/s11252-017-0710-1.
Kormann, R., Meixner, F.X., 2001. An analytical footprint model for non-neutral stratification. Boundary-Layer Meteorol. 99, 207–224.
Kotthaus, S., Grimmond, C.S.B., 2012. Identification of micro-scale anthropogenic CO2, heat and moisture sources–processing eddy covariance fluxes for a dense urban environment. Atmos. Environ. 57, 301–316.
Kotthaus, S., Grimmond, C.S.B., 2014a. Energy exchange in a dense urban environment–Part I: temporal variability of long-term observations in central London. Urban Clim. 10, 261–280.
Kotthaus, S., Grimmond, C.S.B., 2014b. Energy exchange in a dense urban environment–Part II: impact of spatial heterogeneity of the surface. Urban Clim. 10, 281–307.
Kotthaus, S., Grimmond, C.S.B., 2017. Characterising London's Urban Boundary Layer Based on Ceilometer Observations (in prep).
Lane, S., Barlow, J.F., Wood, C.R., 2013. An assessment of a three-beam Doppler lidar wind profiling method for use in urban areas. J. Wind Eng. Ind. Aerodyn. 119, 53–59.
Leclerc, M.Y., Foken, T., 2014. Footprints in Micrometeorology and Ecology. Springer, Berlin, p. 239.
Li, Q., Zhi, L., Hu, F., 2010. Boundary layer wind structure from observations on a 325m tower. J. Wind Eng. Ind. Aerodyn. 98, 818–832.
Liu, J., Gao, Z., Wang, L., Li, Y., Gao, C.Y., 2017. The impact of urbanization on wind speed and surface aerodynamic characteristics in Beijing during 1991–2011. Meteorol. Atmos. Phys. 1–14.
Lindberg, F., Grimmond, C.S.B., 2011. Nature of vegetation and building morphology characteristics across a city: influence on shadow patterns and mean radiant temperatures in London. Urban Ecosyst. 14, 617–634.
Macdonald, R., Griffiths, R., Hall, D., 1998. An improved method for the estimation of surface roughness of obstacle arrays. Atmos. Environ. 32, 1857–1864.
Macdonald, R.W., Carter, S., Slawson, P.R., 2000. Measurements of Mean Velocity and Turbulence Statistics in Simple Obstacle Arrays at 1:200 Scale. Thermal Fluids Report. Department of Mechanical Engineering, University of Waterloo, pp. 2000–2001.
Mahrt, L., 1998. Nocturnal boundary-layer regimes. Boundary-Layer Meteorol. 88, 255–278.
Mahrt, L., 2000. Surface heterogeneity and vertical structure of the boundary layer. Boundary-Layer Meteorol. 96, 33–62.
Millward-Hopkins, J., Tomlin, A., Ma, L., Ingham, D., Pourkashanian, M., 2013. Assessing the potential of urban wind energy in a major UK city using an analytical model. Renew. Energy 60, 701–710.
Miyake, M., 1965. Transformation Ofthe Atmospheric Boundary Layer over Inhomogeneous Surfaces. Scientific report. University of Washington, Seattle, p. 63.
Mohammad, A.F., Zaki, S.A., Ali, M.S.M., Aya, H., Razak, A.A., Shirakashi, M., Arai, N., 2015. Large Eddy Simulation of wind pressure distribution on heterogeneous buildings in idealised urban models. Energy Procedia 78, 3055–3060.
Oke, T.R., 2007. Siting and exposure of meteorological instruments at urban sites. In: Borrego, C., Norman, A.L. (Eds.), Air Pollution Modelling and its Application XVII. Springer, USA, p. 744.
Peña, A., Gryning, S., Mann, J., Hasager, C.B., 2010. Length scales of the neutral wind profile over homogeneous terrain. J. Appl. Meteorol. Climatol. 49, 792–806.
Petrini, F., Ciampoli, M., 2012. Performance-based wind design of tall buildings. Struct. Infrastruct. Eng. 8, 954–966.
Raupach, M., Antonia, R., Rajagopalan, S., 1991. Rough-wall turbulent boundary layers. Appl. Mech. Rev. 44, 1–25.
Ricci, A., Kalkman, I., Blocken, B., Burlando, M., Freda, A., Repetto, M.P., 2016. Inflow condition sensitivity in the CFD simulation of wind flow in the urban environment. In: International Colloquium on Bluff Body Aerodynamics and Applications, p. 2016. Boston, Massachusetts, USA, June 7 – 11.
Roth, M., 2000. Review of atmospheric turbulence over cities. Q. J. R. Meteorol. Soc. 126, 941–990.
Savelyev, S.A., Taylor, P.A., 2005. Internal boundary layers: I. Height formulae for neutral and diabatic flows. Boundary-Layer Meteorol. 115, 1–25.
Schultz, M., Schatzmann, M., Leitl, B., 2005. Effect of roughness inhomogeneities on the development of the urban boundary layer. Int. J. Environ. Pollut. 25, 105–117.
Sedefian, L., 1980. On the vertical extrapolation of mean wind power density. J. Appl. Meteorol. 19, 488–493.
Segal, M., Pielke, R.A., 1988. The extrapolation of vertical profiles of wind speed within the marine atmospheric surface layer using the p formula. J. Appl. Meteorol. 27, 174–181.
Seidel, D.J., Ao, C.O., Li, K., 2010. Estimating climatological planetary boundary layer heights from radiosonde observations: comparison of methods and uncertainty analysis. J. Geophys. Res. Atmos. 115, D16113.
Tamura, Y., Suda, K., Sasaki, A., Iwatani, Y., Fujii, K., Ishibashi, R., Hibi, K., 2001. Simultaneous measurements of wind speed profiles at two sites using Doppler sodars. J. Wind Eng. Ind. Aerodyn. 89, 325–335.
Tan, J., Yang, L., Grimmond, C., Shi, J., Gu, W., Chang, Y., Hu, P., Sun, J., Ao, X., Han, Z., 2015. Urban integrated meteorological observations: practice and experience in Shanghai, China. Bull. Am. Meteorol. Soc. 96, 85–102.
Tanaka, H., Tamura, Y., Ohtake, K., Nakai, M., Kim, Y.C., 2012. Experimental investigation of aerodynamic forces and wind pressures acting on tall buildings with various unconventional configurations. J. Wind Eng. Ind. Aerodyn. 107, 179–191.
Taranath, B.S., 2016. Structural Analysis and Design of Tall Buildings: Steel and Composite Construction. CRC Press, Florida, p. 722.
Tennekes, H., 1973. The logarithmic wind profile. J. Atmos. Sci. 30, 234–238.
Tominaga, Y., Stathopoulos, T., 2016. Ten questions concerning modeling of near-field pollutant dispersion in the built environment. Build. Environ. 105, 390–402.
Tsuang, B., Tsai, J., Lin, M., Chen, C., 2003. Determining aerodynamic roughness using tethersonde and heat flux measurements in an urban area over a complex terrain. Atmos. Environ. 37, 1993–2003.
Walmsley, J., Taylor, P., Keith, T., 1986. A simple model of neutrally stratified boundary-layer flow over complex terrain with surface roughness modulations (MS3DJH/3R). Boundary-Layer Meteorol. 36, 157–186.
Walmsley, J.L., Woolridge, D., Salmon, J.R., 1990. Ms-Micro/3 User's Guide. Technical Report ARD-90-008. Atmospheric Environment Services, Ontario, Canada, p. 88.
Wang, K., Stathopoulos, T., 2007. Exposure model for wind loading of buildings. J. Wind Eng. Ind. Aerodyn. 95, 1511–1525.
Wieringa, J., 1986. Roughness-dependent geographical interpolation of surface wind speed averages. Q. J. R. Meteorol. Soc. 112, 867–889.
Wieringa, J., 1993. Representative roughness parameters for homogeneous terrain. Boundary-Layer Meteorol. 63, 323–363.
Wilson, J.D., Flesch, T.K., 2003. Wind measurements in a square plot enclosed by a shelter fence. Boundary-Layer Meteorol. 109, 191–224.
Wood, C.R., Pauscher, L., Ward, H., Kotthaus, S., Barlow, J., Gouvea, M., Lane, S., Grimmond, C.S.B., 2013. Wind observations above an urban river using a new lidar technique, scintillometry and anemometry. Sci. Total Environ. 442, 527–533.
Xie, Z., Coceal, O., Castro, I.P., 2008. Large-eddy simulation of flows over random urban-like obstacles. Boundary-Layer Meteorol. 129, 1–23.
Yang, X.I., Sadique, J., Mittal, R., Meneveau, C., 2016. Exponential roughness layer and analytical model for turbulent boundary layer flow over rectangular-prism roughness elements. J. Fluid Mech. 789, 127–165.
Zaki, S.A., Hagishima, A., Tanimoto, J., Ikegaya, N., 2011. Aerodynamic parameters of urban building arrays with random geometries. Boundary-Layer Meteorol. 138, 99–120.
Zhang, X., Zhang, R.R., 2001. Actual ground-exposure determination and its influences in structural analysis and design. J. Wind Eng. Ind. Aerodyn. 89, 973–985.
Zoumakis, N.M., 1993. Estimating the zero-plane displacement and roughness length for tall vegetation and forest canopies using semi-empirical wind profiles. J. Appl. Meteorol. 32, 574–579.